Qualification of Nuclear Design Methodology using PARAGON/ANC

Non-Proprietary Version

December 2007

Page Intentionally Left Blank

Revision History

Revision	Page	Description
0	All	Original issued

Abstract

This document presents the qualification of Mitsubishi Heavy Industries, LTD. PWR's nuclear design methodology using PARAGON/ANC. The qualification of MHI PWR nuclear design method using PARAGON/ANC has been performed by comparing the code system results with measurement data from critical experiments, Post-Irradiation Examination and operating plants. As a result of these analyses, the good performance of the PARAGON/ANC code system demonstrates the ability of the MHI to apply PWR nuclear design methodology using PARAGON/ANC.

Table of Contents

List of Tables

List of Figures

List of Acronyms

APWR	Advanced Pressurized Water Reactor
ARO	All Rods Out
BOC	Beginning of Cycle
B&W	Babcock & Wilcox Spatial Criticals
B/N	Belgonucléaire
EOC	End of Cycle
HFP	Hot Full Power
HZP	Hot Zero Power
MHI	Mitsubishi Heavy Industries, LTD.
MOC	Middle of Cycle
MOX	Mixed Oxide Fuel
NEM	Nodal Expansion Method
PIE	Post-Irradiation Examination
PWR	Pressurized Water Reactor
SCK/CEN	Belgian Nuclear Research Center
STD	Standard Deviation
TCA	Tank-type Critical Assembly
US NRC	United States Nuclear Regulatory Commission
VIP	Venus International Program
WH	Westinghouse Electric Company, LLC.

1.0   INTRODUCTION

This document presents the qualification of Mitsubishi Heavy Industries, LTD. (MHI) PWR's nuclear design methodology using PARAGON/ANC.

PARAGON/ANC (References 1, 2, 3) is a PWR nuclear design code system developed by Westinghouse Electric Company, LLC. (WH). The code system application to PWRs core design has been previously approved by the US NRC. The purpose of the document is to demonstrate the ability of MHI to use the code system. PARAGON is mainly used for generating group constants for the core simulator ANC based on a multi group heterogeneous two dimensional transport assembly calculation. ANC is used for evaluating the main nuclear core parameters, such as power distribution, fuel burnup, critical boron concentration, doppler and moderator reactivity coefficients, based on a three dimensional two-group diffusion theory methodology. MHI introduced this code system from WH and it has been using in the nuclear analysis of Japanese PWRs. Furthermore, since the 1990s and for over 10 years, MHI and WH have implemented joint development programs in order to make a further methodology development and improvement of this code system. Therefore, MHI has experience both in the use and in the development of the code system.

MHI has constructed 23 Westinghouse type standard PWR plants in Japan since the 1970s. Additionally, MHI has experience in the design of over 400 reload cores, including 19 initial cores. MHI experience in construction, design and reload includes 2 loop plants with 121 assemblies, 3 loop plants with 157 assemblies and 4 loop plants with 193 assemblies, with 14x14, 15x15 and 17x17 fuel assembly lattice configurations. MHI has implemented different burnup extension programs which allow a maximum fuel rod burnup increase from 43,000 MWD/MTU in the 1970s to the current limit of 62,000 MWD/MTU. MHI also has extensive experience with PYREX and Gadolinia burnable absorbers. Additionally, for extended burnup reload cores, fuel assemblies with 4.8 wt% Uranium enrichment fuel rods and 10 wt% Gadolinia content fuel rods has been designed in recent years. In consequence, MHI has enough experience in improving the nuclear performance of PWRs.

In order to qualify the MHI PWR nuclear design methodology, this document summarizes the results obtained for Japanese and overseas critical experiments, Post-Irradiation Examination (PIE) and operating plant analysis with PARAGON and PARAGON/ANC. The structure of this document is as follows.

- ・ Chapter 2 describes briefly the theory of PARAGON/ANC.
- ・ Chapter 3 describes the results of applying this code system to critical experiments, PIE results and operating plants.
- ・ The conclusions of this qualification report are summarized in Chapter 4.

2.0 PARAGON/ANC DESCRIPTION

The applicability of PARAGON/ANC to PWR nuclear design was already approved by US NRC, and the code system is used and accepted in the nuclear industry in the United States and also worldwide. The methodology and qualification of PARAGON is described in Reference 1. In Reference 2, the methodology of ANC is described. The qualification of ANC is described in both References 1 and 3.

PARAGON is a lattice physics code. It models a heterogeneous two-dimensional assembly based on current coupling collision probability method. The effective cross sections of each nuclide included in each region of a heterogeneous assembly are generated from a multi-group cross section library based on material composition, configuration, temperature, and other assembly specification data. The 70 energy group library is mainly based on ENDF/B-VI files. The fine energy group neutron spectrum of each region in the heterogeneous assembly is calculated with current coupling collision probability method. Then, the critical spectrum is calculated with a B1 leakage calculation. The B1 spectrum is used to normalize the flux distribution from the two-dimensional transport calculation, and the group constants for ANC are generated by collapsing the assembly group constants with the neutron spectrum. In the PARAGON depletion calculation, the differential equations of the composition changes due to isotopic depletion and buildup in each region of the assembly are solved to evaluate the isotopic composition change using Laplace transformation technique. Additionally, the predictor-corrector method is used for accurate evaluation of composition change.

ANC is a core simulator code. It is a three-dimensional two-group diffusion core calculation code based on a nodal expansion method (NEM). Using few-group constants generated by PARAGON, ANC calculates critical boron concentration, power distribution, fuel burnup, reactivity coefficients, core stability, and other nuclear parameters. Discontinuity factors are used for cross section homogenization correction and a pin power reconstruction method is used for calculating the pinwise power distribution. Nuclides which have a large impact on group constants, such as Xenon and Samarium, are treated explicitly in group constants. The decay, depletion and buildup of these nuclides are evaluated using the local power history and the subsequent effects on group constants are considered in ANC calculation.

3.0   CALCULATION RESULTS OF PARAGON/ANC

3.1   Critical Experiments and Post-Irradiation Examination Analysis

As mentioned in Chapter 2, PARAGON is used to generate few group constants for ANC. In this section, the results obtained for domestic and overseas critical experiments and PIE analyses with PARAGON are discussed in order to show the MHI's PARAGON calculation accuracy to generate group constants and to calculate nuclide composition change with depletion.

In addition, due to the fact that the US-APWR employs a steel neutron reflector instead of conventional baffle reflector for neutron economy and vessel irradiation reduction, the accuracy of the neutron reflector cross sections for ANC based on one dimensional PARAGON model is also discussed here. Compared to the conventional baffle reflector, the thickness of stainless steel is increased, while the coolant area of the outer core region is decreased. To confirm the applicability of PARAGON to generate few group constants for the neutron reflector to be used in the core calculations, a critical experiment benchmark using an iron neutron reflector was performed. The experiment was carried out in the Tank-type Critical Assembly (TCA) in Japan. The results of PARAGON calculations compared to the iron reflector experiment are also shown in this chapter and the applicability of PARAGON for the neutron reflector constants calculation is confirmed.

The rest of this section is organized as follows. Section 3.1.1 describes the results of the critical experiments. In Section 3.1.2, the results of PIE analysis is described. The results of the iron reflector experiment are then described in Section 3.1.3.

3.1.1   Critical Experiments

As shown in Reference 1, PARAGON calculations of Strawbridge-Barry 101 Criticals (Reference 4), KRITZ High-Temperature Criticals (Reference 5) and Babcock & Wilcox Spatial Criticals (B&W) (Reference 6, 7) were performed. A comparison with the Monte Carlo code MCNP (Reference 8) calculation was also made for the qualification of PARAGON in Reference 1.

The Strawbridge-Barry 101 Criticals are uniform lattice critical experiments with several lattice

parameters such as water to Uranium ratio, enrichment, experimental buckling, pellet diameter, and boron concentration. As shown in Reference 1, The agreement between PARAGON calculated results and measurements is excellent and there are neither biases nor particular trends with these lattice parameters.

The KRITZ High-Temperature Criticals are critical experiments for high temperature condition with UO$_2$ fuel. As shown in Reference 1, The agreement between PARAGON calculated results and measurements is excellent and there is no particular tendency of the calculation and measurements difference with the temperature range.

The Babcock & Wilcox Spatial Criticals are critical experiments for a variety of lattice configurations such as PYREX rods, Gadolinia rods, control rods, and water holes with UO$_2$ fuel rods. Both reactivity and power distribution are measured and compared to PARAGON calculation. As shown in Reference 1, The agreement between PARAGON calculated results and measurements is excellent for both reactivity and power distribution, and there is no particular tendency of the calculation and measurement difference with the variety lattice configurations.

To supplement the PARAGON results in Reference 1, MHI has also performed B&W critical experiments (Reference 6, 7, 9) not reported in Reference 1 and the Venus International Program (VIP) (Reference 10) critical experiments analyses using PARAGON in addition to the above critical experiments. PARAGON results for these additional experiments are reported in sections 3.1.1.1 and 3.1.1.2, respectively.

3.1.1.1   Babcock & Wilcox Spatial Critical Experiments

As described in references 6, 7 and 9, in the B&W critical experiments, reactivity and power distributions were measured for typical PWR lattice configurations. The core configuration is shown in Figure 3.1-1. The critical experiments include various lattice configurations, guide thimble patterns and several burnable absorber patterns such as PYREX and Gadolinia rods. The enrichment of UO$_2$ fuel rods are 2.46 wt% and 4.02 wt%, and the Gadolinia content is 4.00 wt%.

The description of the B&W critical experiments not included in Reference 1 but analyzed by MHI with PARAGON is shown in Table 3.1-1. The 15x15 lattice configuration is used in Core XI. The power distribution comparison between the measurement and PARAGON calculation for

the center assembly is shown in Table 3.1-2, Figure 3.1-2 through Figure 3.1-4. As shown in this table and these figures, the agreement between PARAGON calculated and measured rod powers is excellent. The maximum rod power difference within [   ], but the vast majority of pin powers is within [   ].

3.1.1.2   Venus International Program (VIP) Critical Experiments

The VIP critical experiments were mainly conducted by Belgonucléaire (B/N) and the Belgian Nuclear Research Center (SCK/CEN). Reactivity and power distribution were measured for the PWR 17x17 lattice configuration shown in Figure 3.1-5. The critical experiment layout consists on a MOX fuel assembly surrounded by 4 UO_2 fuel assemblies. The UO_2 assembly's Uranium enrichment is 3.0 wt%. The MOX fuel assembly has rods with three different Plutonium total contents. The total Plutonium contents are 12.6 wt% for the high-content MOX rods, 8.6 wt% for the medium-content MOX rods and 4.8 wt% for the low-content MOX fuel. These fuel assemblies are surrounded by a driver fuel region with 3.0 wt% and 4.0 wt% UO_2 fuel rods.

For the reactivity comparison, the PARAGON eigenvalue was compared with the measured critical eigenvalue, i.e. 1.0. The [   ] eigenvalue obtained with PARAGON shows good agreement with the measurement, with a discrepancy of only about [   ]. The fuel rod power distributions in the center assemblies obtained with PARAGON were compared with the measurements based on gamma scan. The power distribution differences between PARAGON and measurement results for the MOX and UO_2 fuel assemblies are shown in Figure 3.1-6 and Figure 3.1-7, respectively. These figures show that the agreement between PARAGON calculated rod powers and measurements is excellent with the maximum rod power difference is within [   ]. The standard deviations of the relative difference of fuel rod power distribution are [   ] for MOX fuel and [   ] for UO_2 fuel, respectively.

3.1.2   Post-Irradiation Examination

In order to qualify the use of PARAGON for nuclide composition changes with depletion, PARAGON calculation results were compared with isotopic data from Saxton and Yankee's PIE analysis, as shown in Reference 1. The measured isotopic data for Saxton and Yankee's fuel rods were compared to PARAGON calculation results. There is no significant trend between PARAGON calculated results and measurements for any isotope with burnup.

In addition to this PIE analysis, MHI has used PARAGON to analyze Goesgen, Beznau, Takahama, and BR3 PIE measurements, as described in the next sections.

3.1.2.1   UO$_2$ and MOX Fuel

The PIE data were obtained from discharged fuel assemblies of Takahama, Goesgen and Beznau PWRs (Reference 11, 12). The descriptions of these PIE data are shown in Table 3.1-3. As can be seen from this table, PIEs were performed for UO$_2$ and MOX fuel. The enrichment ranged from 3.5 wt% to 4.1 wt% and the fissile Pu content was about 6 wt%. The maximum sample burnup in the PIE is about 59GWd/t for UO$_2$ fuel and about 56GWd/t for MOX fuel.

The Uranium and Plutonium isotope contents comparison between PARAGON calculations and measurements are shown in Figure 3.1-8 and Figure 3.1-9 and demonstrate very good results. The comparison of the Plutonium isotopes of UO$_2$ fuel has relatively large differences compared to the Uranium isotopes since the contents of Plutonium isotopes are significantly smaller than the Uranium isotopes content. However, the discrepancies between PARAGON results and measurements are independent from fuel type and burnup. As a result of these analyses, the good performance of the PARAGON code demonstrates the ability to predict the depletion characteristics for both UO$_2$ and MOX fuel.

3.1.2.2   High Content Gadolinia Fuel

High content Gadolinia fuel, with Gadolinia contents of 7 wt% and 10 wt%, were irradiated in the European irradiation test reactor BR3 and PIE for obtaining the Gadolinium isotope contents with burnup were performed (Reference13). The [155]Gd and [157]Gd content change with burnup for 7 wt% and 10 wt% Gadolinia fuel are shown in Figure 3.1-10 and Figure 3.1-11, respectively. As shown in these figures, PARAGON calculations show good agreement with measurements within the experimental error. No particular tendency between PARAGON calculation and PIE results is found. As a result of these analyses, the good performance of the PARAGON code demonstrates the ability of PARAGON to correctly predict high content Gadolinia fuel.

3.1.3   Critical Experiments with Iron Neutron Reflector

As has been noted above, the US-APWR employs a steel neutron reflector (called neutron

reflector) instead of a conventional baffle reflector for the purpose of neutron economy improvement and vessel irradiation reduction. To confirm the applicability of PARAGON for the neutron reflector, critical experiments were performed in TCA using an iron reflector (Reference 14, 15).

The TCA critical experiments were carried out to evaluate the reactivity effect of the iron reflector on the PWR lattice configuration. 2.6 wt% UO_2 fuel rods were used for the core. The effects of the thickness of the iron reflector and distance between the core and the iron reflector on reactivity were measured in the experiments. The thickness of iron reflector was varied from a few millimeters to 150mm (5.91inch). The neutron density distributions (epi-thermal and thermal) were also measured for no reflector and 60mm (2.36inch) thickness iron reflector conditions. The neutron density was measured by using relative activation rate of Gold wires.

The effect of iron thickness on the reactivity is reported in References 14 and 15. Comparison of measurement and PARAGON reactivity effect, as a function of the iron reflector thickness, is shown in Figure 3.1-12. As shown in this figure, the agreement of PARAGON calculations and measurements is excellent, within [   ], except for the first few millimeters of reflector thickness, and additionally, no particular tendency of the calculation/measurements difference with the thickness of iron reflector is observed.

The applicability of PARAGON has been demonstrated for the baffle reflector of the operating PWRs in the USA and Japan. These TCA experiments corroborate this applicability since PARAGON shows an excellent agreement for the reflector thickness of approximately 20mm (0.79inch). The US-APWR design uses a neutron reflector thickness which is approximately [   ] to [   ], is not included explicitly in the TCA critical experiments since the thickness of iron reflector was varied up to 150mm (5.91inch). However, as shown in Figure 3.1-12, the predicted reactivity effects of the iron reflector show excellent agreement with measurements for different thicknesses. Therefore, as PARAGON has the same performance for the different reflector thickness, it is applicable for the US-APWR neutron reflector.

The neutron density distribution comparison between the PARAGON calculation and measurement is shown in Figure 3.1-13 through Figure 3.1-16 for non-reflector and 60mm (2.36inch) reflector conditions. In the reflector region, PARAGON calculated neutron density distributions are slightly lower than the measurements, however in the core region, the

agreement of PARAGON calculated neutron density distributions with measurements are good for both non-reflector and 60mm (2.36inch) reflector thickness conditions. There are no particular trends with the thickness of iron reflector.

As described above, in order to confirm the applicability of PARAGON for the neutron reflector, critical experiments were performed in TCA using iron reflector of different thicknesses. Both reactivity effect and neutron density distribution were measured while varying the iron reflector thickness, and the comparison between PARAGON calculation and measurements shows good agreement. As a result of TCA critical experiment analyses, the good performance of the PARAGON demonstrates the ability of PARAGON to be used for the US-APWR neutron reflector.

Based on this analysis, it is concluded that core leakage and peripheral powers can be accurately calculated.

Table 3.1-1   Configuration of B&W Critical Experiments

Core	Loading	Total Number of Fuel Rods	Total Number of Water Holes	Total Number of PYREX Rods	Boron Concentration (ppm)
XI	3	4808	153	0	1337
	5	4808	117	36	1181
	7	4808	81	72	1031

Table 3.1-2   Results of Power Distribution Analysis of B&W Critical Experiments

Core	Loading	Average Error (%)	Standard Deviation (%)
XI	3	[ ]	[ ]
	5	[ ]	[ ]
	7	[ ]	[ ]

Table 3.1-3   Description of PIE Analysis

Plant Name	Takahama Unit 3	Goesgen	BEZNAU Unit 1
Plant type	17x17 3 Loop	17x17 3 Loop	14x14 2 Loop
PIE sample	UO_2	UO_2	MOX
UO_2 enrichment (wt%)	4.1	About 3.5 & 4.1	About 0.2
Initial fissile Pu content (wt%)	---	---	About 6.0
Maximum Local Burnup （GWD/MTU）	About 47	About 59	About 56

Outer Core
2.46 wt% UO2

Water Holes, PYREX
rods, Gadolinia fuel
rods loading region

Inner Core
Core 1, 5, XI, XIV: 2.46 wt% UO2
Core 12, 14: 4.02 wt% UO2

Power distribution
measurement region
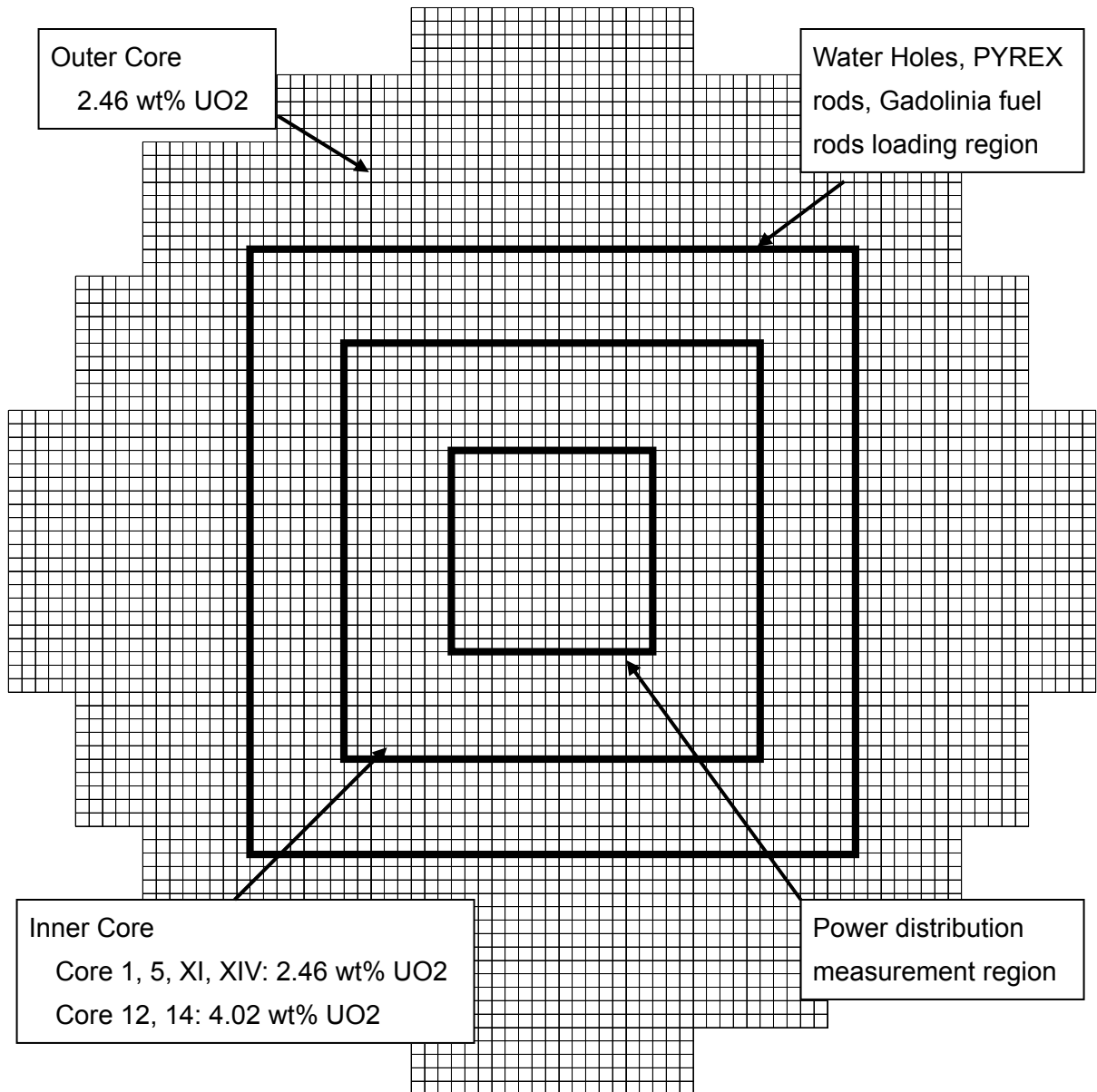
Figure 3.1-1   Core Configuration of B&W Critical Experiment

Figure 3.1-2   Power Distribution of B&W Critical Experiment (Core XI Loading 3)

Figure 3.1-3   Power Distribution of B&W Critical Experiment (Core XI Loading 5)

Figure 3.1-4   Power Distribution of B&W Critical Experiment (Core XI Loading 7)
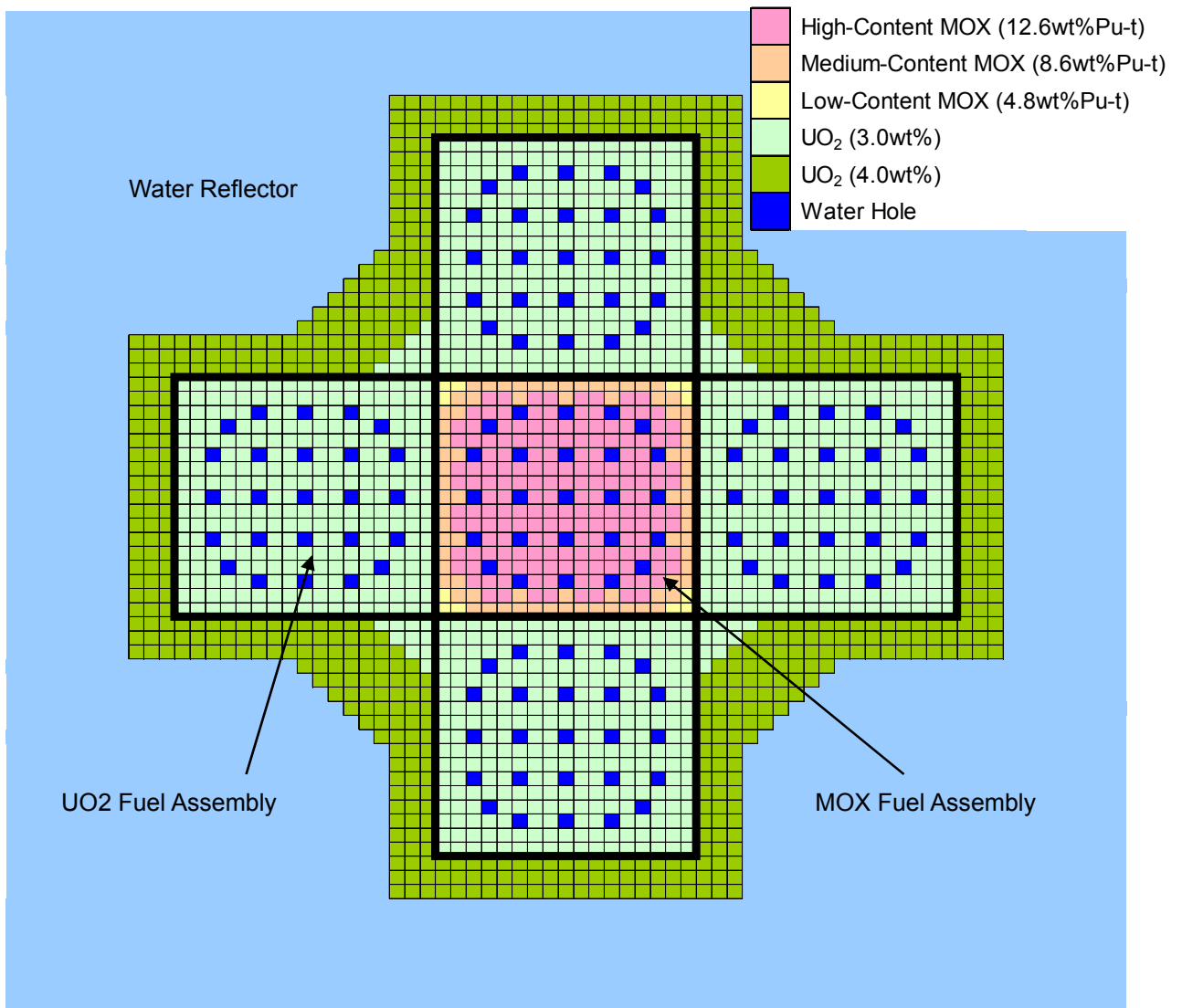
Figure 3.1-5   Core Configuration of VIP Critical Experiment

Figure 3.1-6   Power Distribution of VIP Critical Experiment (MOX Fuel Assembly)

Figure 3.1-7   Power Distribution of VIP Critical Experiment (UO$_2$ Fuel Assembly)

Figure 3.1-8   PIE Analysis (Uranium Isotope)

Figure 3.1-9   PIE Analysis (Plutonium Isotope)
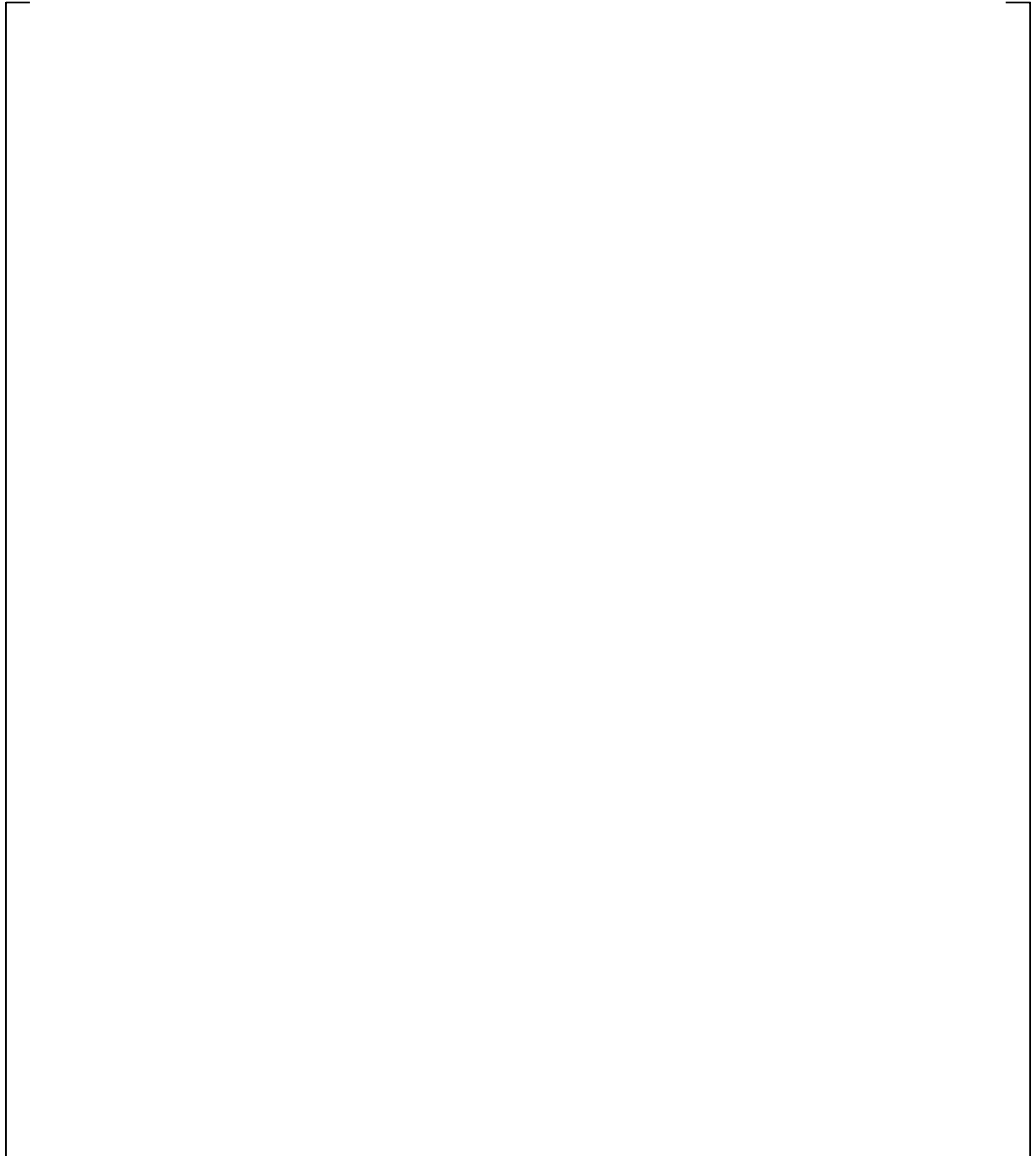
Figure 3.1-10   Gadolinia Isotope Content versus Burnup

(7 wt% Gadolinia Content Fuel)
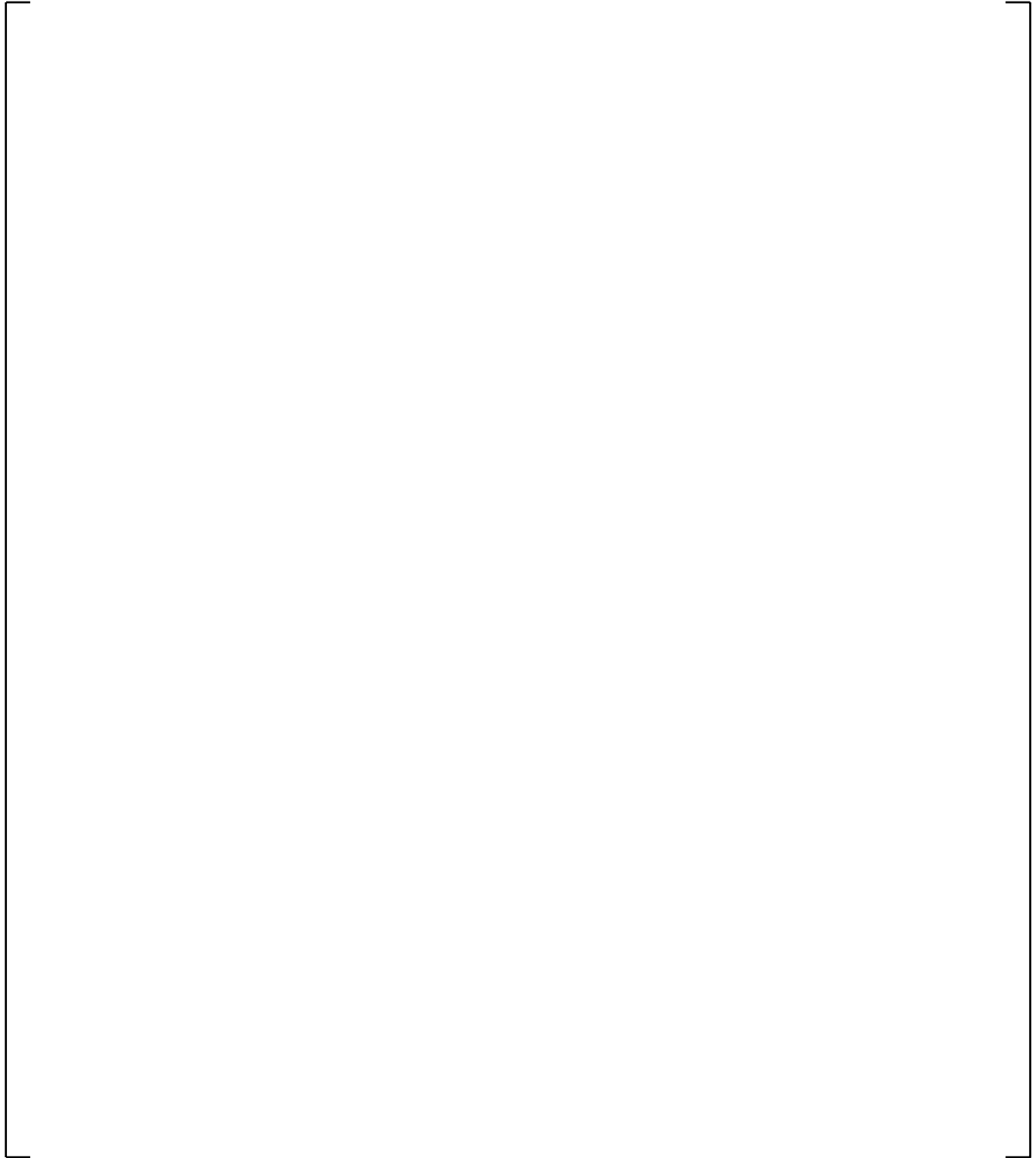
Figure 3.1-11   Gadolinia Isotope Content versus Burnup

(10 wt% Gadolinia Content Fuel)

Figure 3.1-12   Reactivity Effect of Iron Reflector

Figure 3.1-13   Epi-Thermal Neutron Density Distribution (Non-reflector Condition)

Figure 3.1-14   Thermal Neutron Density Distribution (Non-reflector Condition)

Figure 3.1-15   Epi-Thermal Neutron Density Distribution (Reflector Thickness=60mm (2.36inch))

Figure 3.1-16   Thermal Neutron Density Distribution (Reflector Thickness=60mm (2.36inch))

3.2 Operating Plant Analysis

Reference 1 shows PARAGON/ANC calculation results of operating US PWRs as a part of the PARAGON/ANC qualification. In this report, the startup physics tests data and operating plants measurements data for both Westinghouse and Combustion Engineering type PWR plants were compared to PARAGON/ANC calculated results. The agreements between PARAGON/ANC calculated results and measurements are excellent and there are neither biases nor particular trends for plant type, core type, or cycle burnup. In addition, MHI has used Japanese PWR measurement data to demonstrate MHI's ability to apply PARAGON/ANC. The plan of this section is as follows. Subsection 3.2.1 describes the configuration of analyzed cores. In Subsection 3.2.2, the results of startup physics tests are presented. Finally, Subsection 3.2.3 states the results of operating plant data.

3.2.1 Analyzed Core Configuration

The configuration of the cores for the PARAGON/ANC qualification is shown in Table 3.2-1. The Japanese operating PWR plants are Westinghouse type standard PWR. The analysis includes initial and reload cores with high content Gadolinia and extended burnup UO_2 fuel. The analysis includes 10 cycles of 2 plants. One of the plants is a 3 loop plant with 157 assemblies and the other is a 4 loop plant with 193 assemblies. The lattice configuration is a typical 17x17 fuel assembly and the enrichment ranges from 2.0 wt% to 4.8 wt%. PYREX and/or Gadolinia burnable absorbers are used. There are two Gadolinia contents; one is 6.0 wt%, and the other is 10.0 wt%, while the number of Gadolinia rods per assembly is 16 and 24 rods for 6.0 wt% and 10.0 wt%, respectively.

3.2.2 Startup Physics Tests

The comparison of BOC HZP startup physics tests measurement data (critical boron concentration, isothermal temperature coefficient, and control rod worth) with PARAGON/ANC calculation are shown in Figure 3.2-1 through Figure 3.2-3. The comparison contains results for 10 cores, including 1st cycle, 2nd cycle and 3 equilibrium reload cores for each plant. Some of the results of critical boron concentration and isothermal temperature coefficient for 1st and 2nd cycles include rodded condition results such as D-in, DC-in, DCB-in, and DCBA-in. The measured and predicted Bank-D and C control rod worth are compared for all analyzed cores. The differences between PARAGON/ANC calculated results and measurements include uncertainties associated with calculational methods, measurements, manufacturing tolerances

of reactor components, and other terms.

The startup physics tests measurement data were obtained following startup physics tests procedure. The critical boron concentrations are measured at bite position. Next, the control rods are withdrawn to ARO position and then the reactivity change is measured by a reactivity meter. The reactivity change is converted to an equivalent boron concentration by dividing it by the calculated boron worth and is added to the above measured critical boron concentration. The value of the isothermal temperature coefficient is obtained by changing the inlet temperature and measuring the reactivity change. For the measurement of the control rod worth, Dynamic Rod Worth Measurement (DRWM) or the dilution/boration method is used. DRWM method inserts the control rod continuously without boron concentration change and measures the reactivity change. The dilution/boration method changes the boron concentration continuously and compensates the reactivity change by the control rod. The reactivity change is measured by a reactivity meter.

As shown in Figure 3.2-1 through Figure 3.2-3 PARAGON/ANC calculations agree well with startup measurements. For critical boron concentration, Figure 3.2-1, the maximum difference is [   ], the average difference is [   ], and the standard deviation is [   ]. For isothermal temperature coefficients, Figure 3.2-2, the maximum difference is [   ], the average difference is [   ], and the standard deviation is [   ]. Finally, for control rod worth, Figure 3.2-3, the maximum difference is [   ], the average difference is [   ], and the standard deviation is [   ]. These startup physics tests results satisfied the startup physics tests criteria of ANSI-ANS-19.6.1-2005 (Reference 16), and there are no particular trends with the plant type and core. These comparisons of startup physics tests with MHI PWR nuclear design methodology using PARAGON/ANC essentially show the equivalent qualities to the qualification results of Reference 1.

In Japanese PWRs, Xe oscillation tests are performed as part of the startup physics tests of the initial core. A Xe power distribution oscillation is induced by a perturbation to the normal condition by inserting and withdrawing a control rod. The time-dependent radial power tilt was measured in these tests. The comparison of radial power tilt measurement data with PARAGON/ANC calculation is shown in Figure 3.2-4. The predicted and measured stability index is also shown in this figure. It can be seen that the agreement between PARAGON/ANC calculations and measurements is excellent. The agreement for the both amplitude and period of Xe oscillation is good.

3.2.3 HFP Operating Measurement Data

3.2.3.1 Critical Boron Concentration Versus Burnup

The comparison of the critical boron concentration versus burnup for the last 3 cycles of each plant listed in Table 3.2-1 is shown in Figure 3.2-5 through Figure 3.2-10. As can be seen from these figures, the agreement between PARAGON/ANC calculations and measurements is excellent and the burnup dependency is also in good agreement. The soluble ^{10}B depletion is considered in the measurement critical boron concentration.

3.2.3.2 Assembly Power Distribution

The comparisons of the assembly average power distributions, including the standard deviation for each cycle of each plant listed in Table 3.2-1, are shown in Figure 3.2-11 through Figure 3.2-40 at the BOC, MOC and EOC at HFP conditions, respectively. The agreement between PARAGON/ANC calculations and measurements is excellent. Moreover, the maximum difference and standard deviation for all 30 flux maps, corresponding to the BOC, MOC and EOC at HFP conditions of the 10 cycles listed in Table 3.2-1 is [   ] and [   ], respectively. These results of assembly power distribution comparisons satisfy the startup physics tests criteria of ANSI-ANS-19.6.1-2005, and these figures show that there is no particular tendency for plant type, core type, or cycle burnup.

3.2.3.3 Axial Power Distribution

The comparisons of the axial power distribution at the BOC, MOC and EOC at HFP conditions for the last 3 cycles of each plant listed in Table 3.2-1 are shown in Figure 3.2-41 through Figure 3.2-46, respectively. As shown in these figures, there is no particular tendency for plant type and cycle burnup. The agreement between PARAGON/ANC calculations and measurements is excellent.
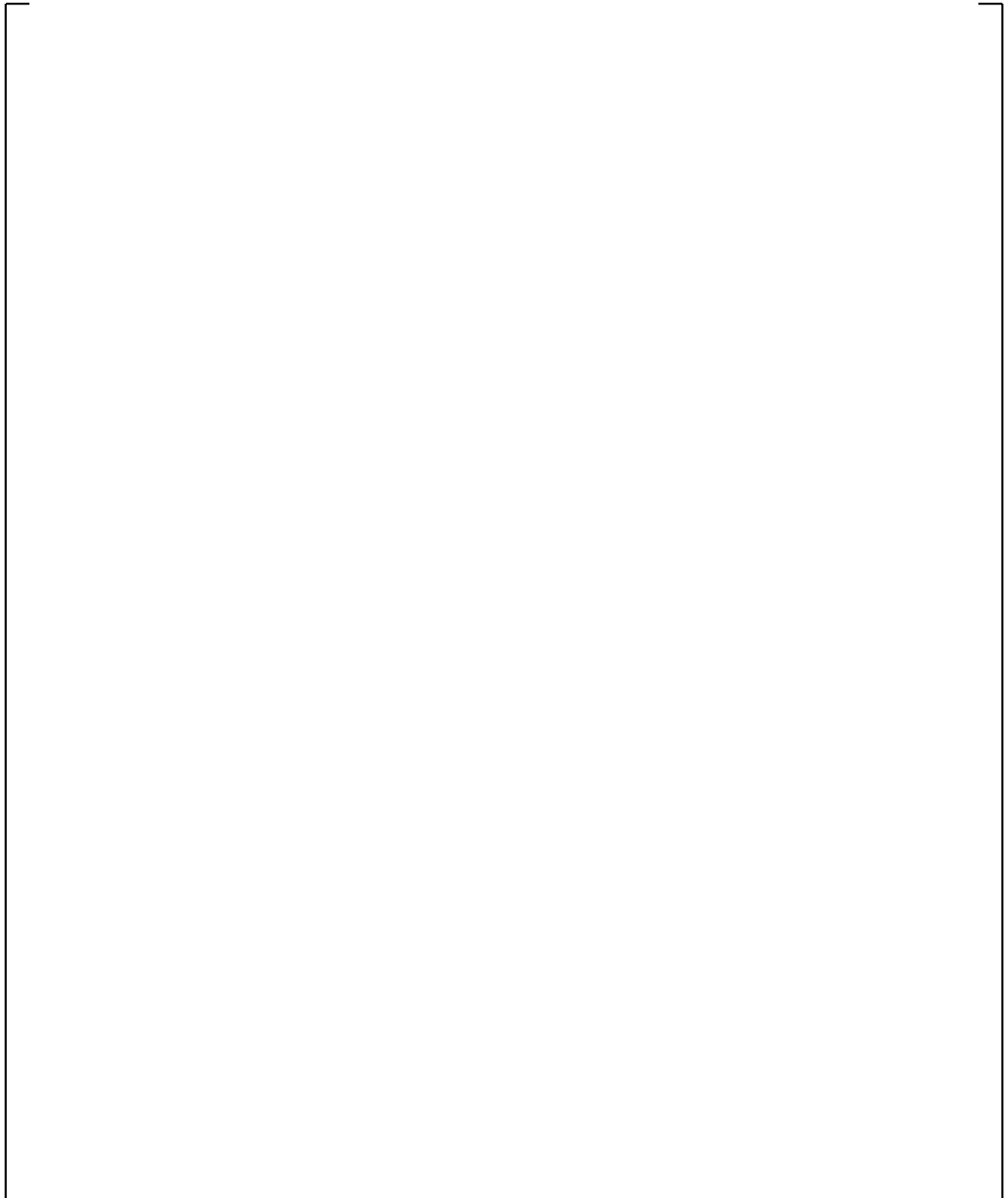
Table 3.2-1   Plant Configuration

Figure 3.2-1   Comparison of Critical Boron Concentration (BOC HZP)

Figure 3.2-2   Comparison of Isothermal Temperature Coefficient (BOC HZP)

Figure 3.2-3   Comparison of Control Rod Worth (BOC HZP)

Figure 3.2-4   Comparison of Radial Power Tilt

(Plant B, During Initial Core Xe Oscillation Test)

Figure 3.2-5   Critical Boron Versus Brunup (Plant A, Cycle 7)

Figure 3.2-6   Critical Boron Versus Brunup (Plant A, Cycle 8)

Figure 3.2-7   Critical Boron Versus Brunup (Plant A, Cycle 9)

Figure 3.2-8   Critical Boron Versus Brunup (Plant B, Cycle 6)

Figure 3.2-9   Critical Boron Versus Brunup (Plant B, Cycle 7)
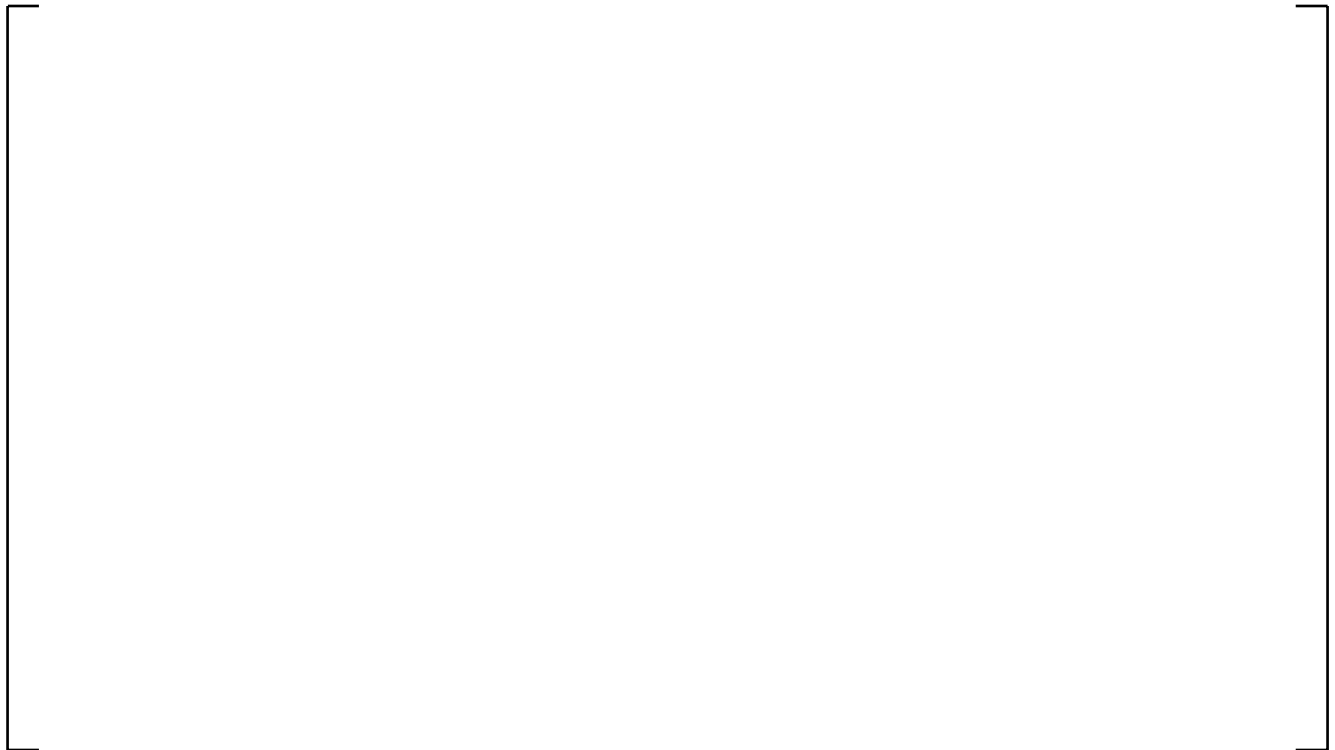
Figure 3.2-10   Critical Boron Versus Brunup (Plant B, Cycle 8)

Figure 3.2-11   Radial Power Distribution (Plant A, Cycle 1, BOC)

Figure 3.2-12   Radial Power Distribution (Plant A, Cycle 1, MOC)

Figure 3.2-13   Radial Power Distribution (Plant A, Cycle 1, EOC)

Figure 3.2-14   Radial Power Distribution (Plant A, Cycle 2, BOC)

Figure 3.2-15   Radial Power Distribution (Plant A, Cycle 2, MOC)
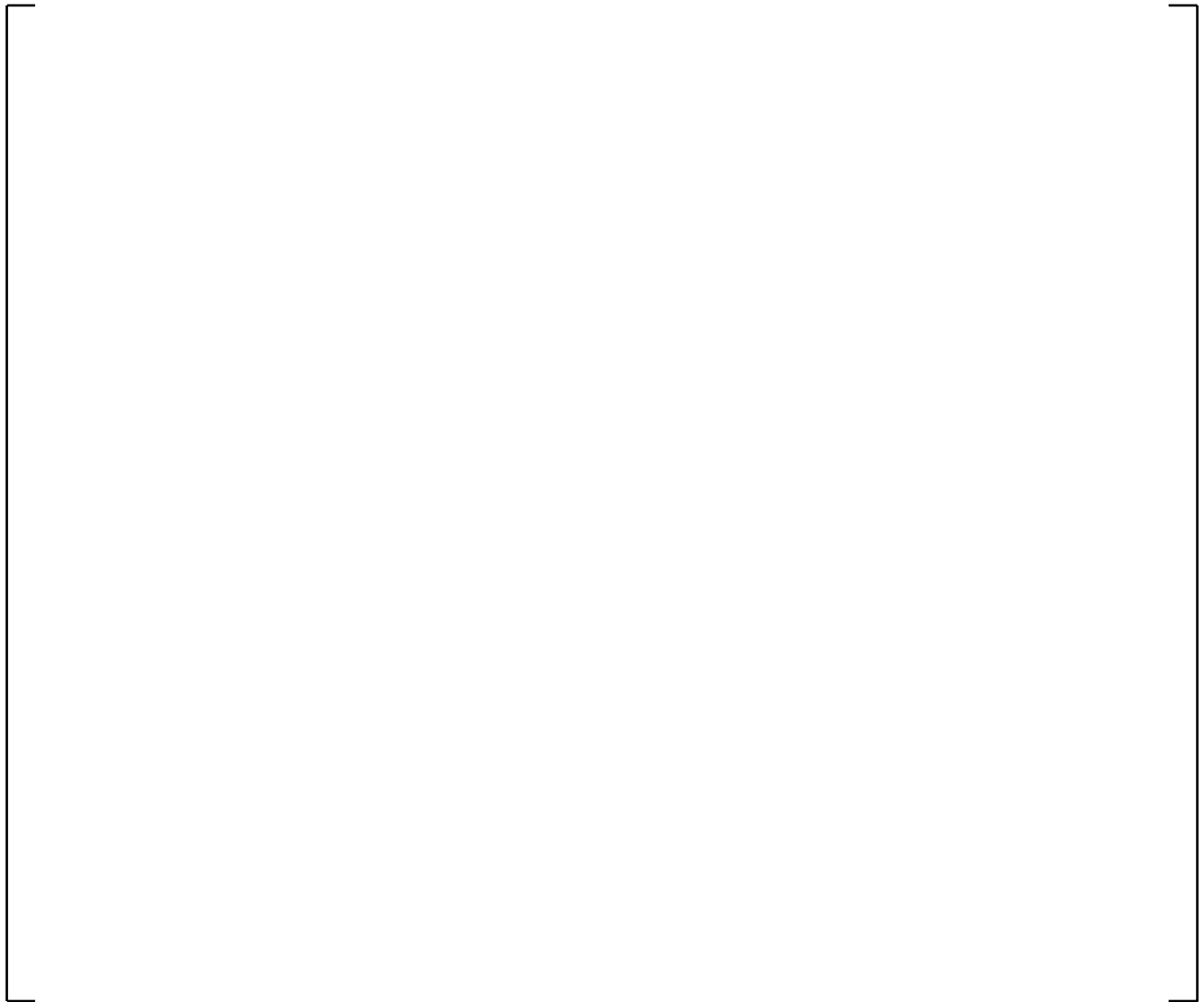
Figure 3.2-16   Radial Power Distribution (Plant A, Cycle 2, EOC)

Figure 3.2-17   Radial Power Distribution (Plant A, Cycle 7, BOC)

Figure 3.2-18   Radial Power Distribution (Plant A, Cycle 7, MOC)

Figure 3.2-19   Radial Power Distribution (Plant A, Cycle 7, EOC)

Figure 3.2-20   Radial Power Distribution (Plant A, Cycle 8, BOC)

Figure 3.2-21   Radial Power Distribution (Plant A, Cycle 8, MOC)

Figure 3.2-22   Radial Power Distribution (Plant A, Cycle 8, EOC)

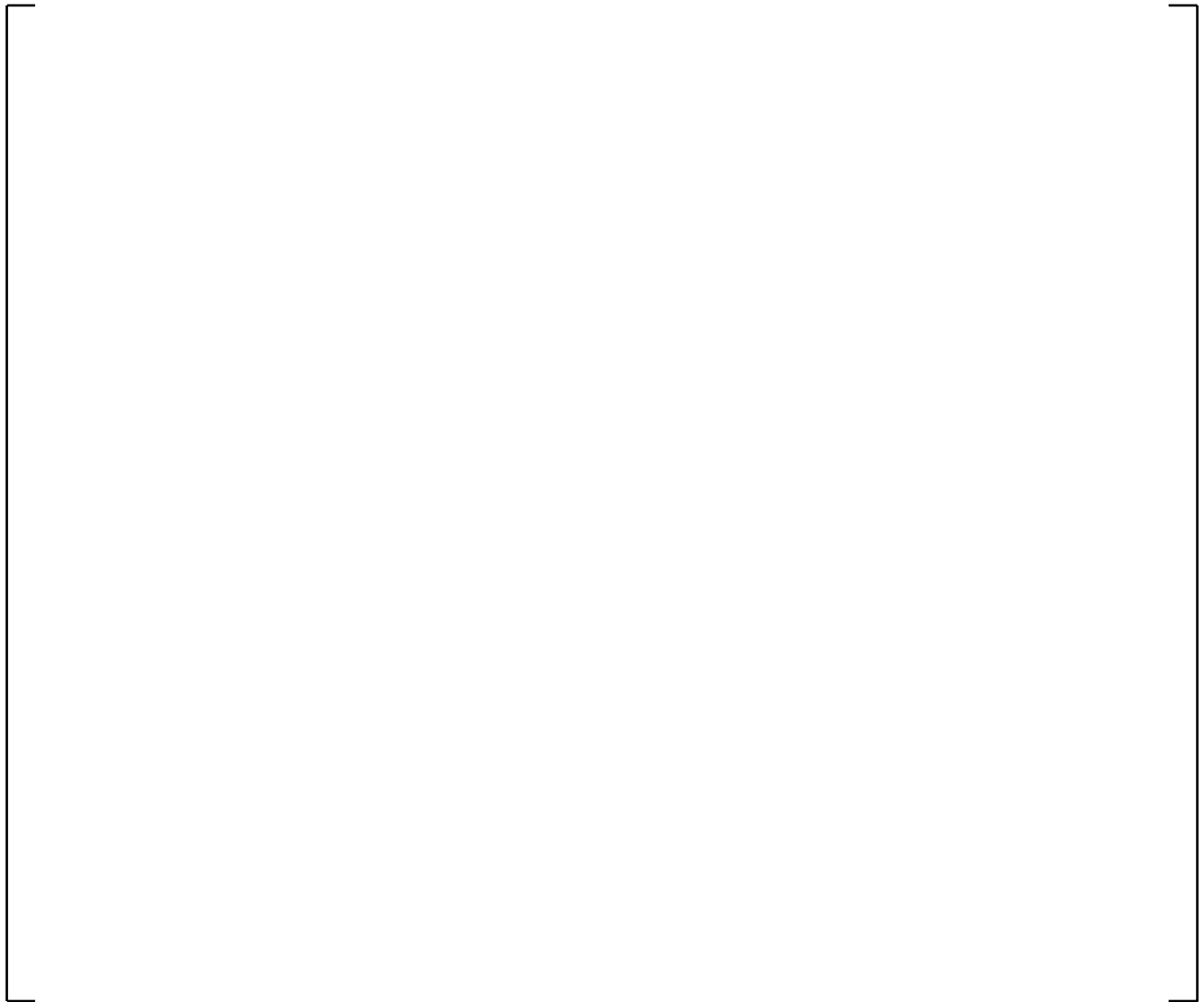**Figure 3.2-23   Radial Power Distribution (Plant A, Cycle 9, BOC)**

Figure 3.2-24   Radial Power Distribution (Plant A, Cycle 9, MOC)

Figure 3.2-25   Radial Power Distribution (Plant A, Cycle 9, EOC)

Figure 3.2-26   Radial Power Distribution (Plant B, Cycle 1, BOC)

Figure 3.2-27   Radial Power Distribution (Plant B, Cycle 1, MOC)

Figure 3.2-28   Radial Power Distribution (Plant B, Cycle 1, EOC)

Figure 3.2-29   Radial Power Distribution (Plant B, Cycle 2, BOC)

Figure 3.2-30   Radial Power Distribution (Plant B, Cycle 2, MOC)

Figure 3.2-31   Radial Power Distribution (Plant B, Cycle 2, EOC)

Figure 3.2-32   Radial Power Distribution (Plant B, Cycle 6, BOC)

Figure 3.2-33   Radial Power Distribution (Plant B, Cycle 6, MOC)

Figure 3.2-34   Radial Power Distribution (Plant B, Cycle 6, EOC)

Figure 3.2-35   Radial Power Distribution (Plant B, Cycle 7, BOC)

Figure 3.2-36   Radial Power Distribution (Plant B, Cycle 7, MOC)

Figure 3.2-37   Radial Power Distribution (Plant B, Cycle 7, EOC)

Figure 3.2-38   Radial Power Distribution (Plant B, Cycle 8, BOC)

Figure 3.2-39   Radial Power Distribution (Plant B, Cycle 8, MOC)

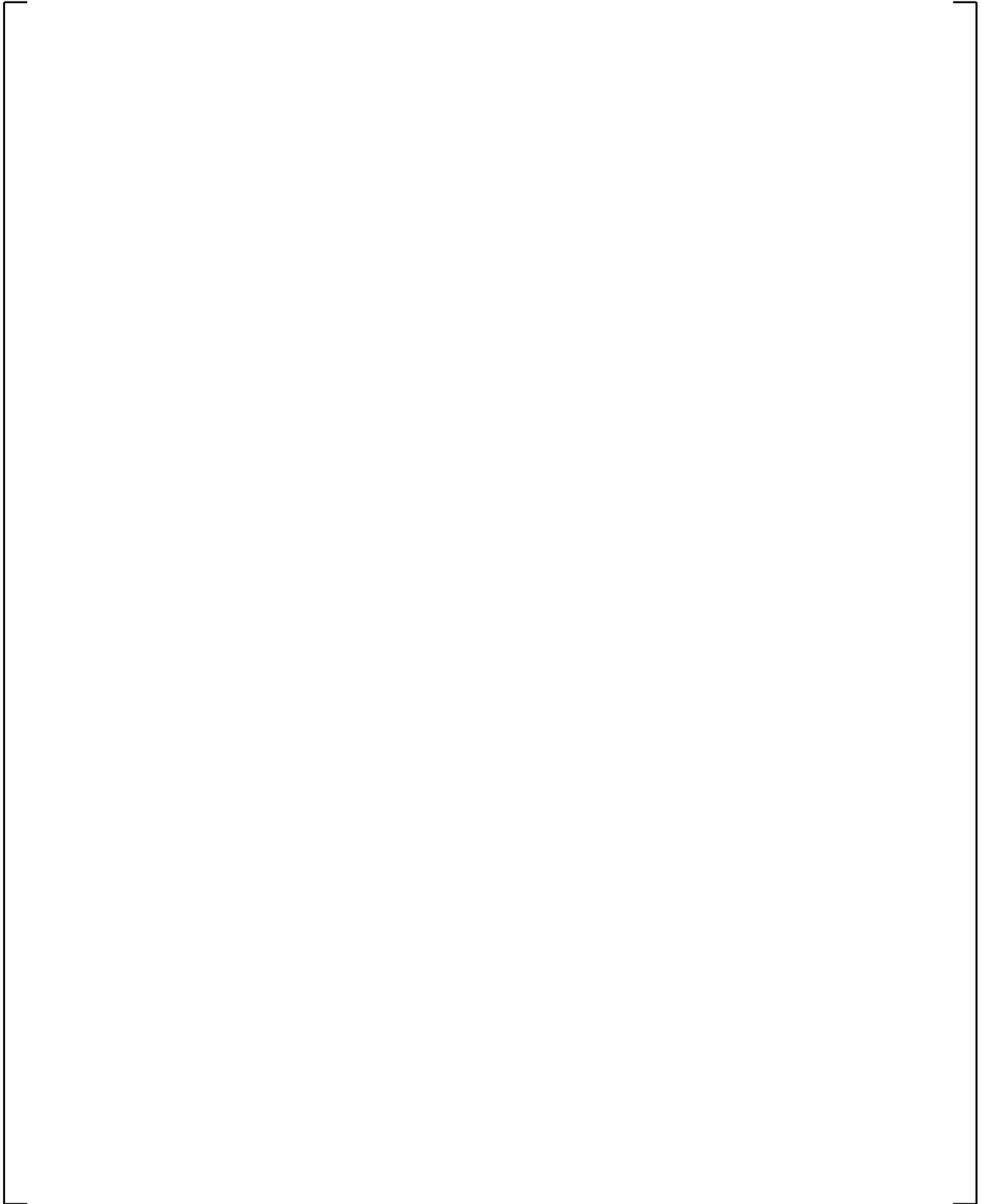**Figure 3.2-40   Radial Power Distribution (Plant B, Cycle 8, EOC)**

Figure 3.2-41   Axial Power Distribution (Plant A, Cycle 7)
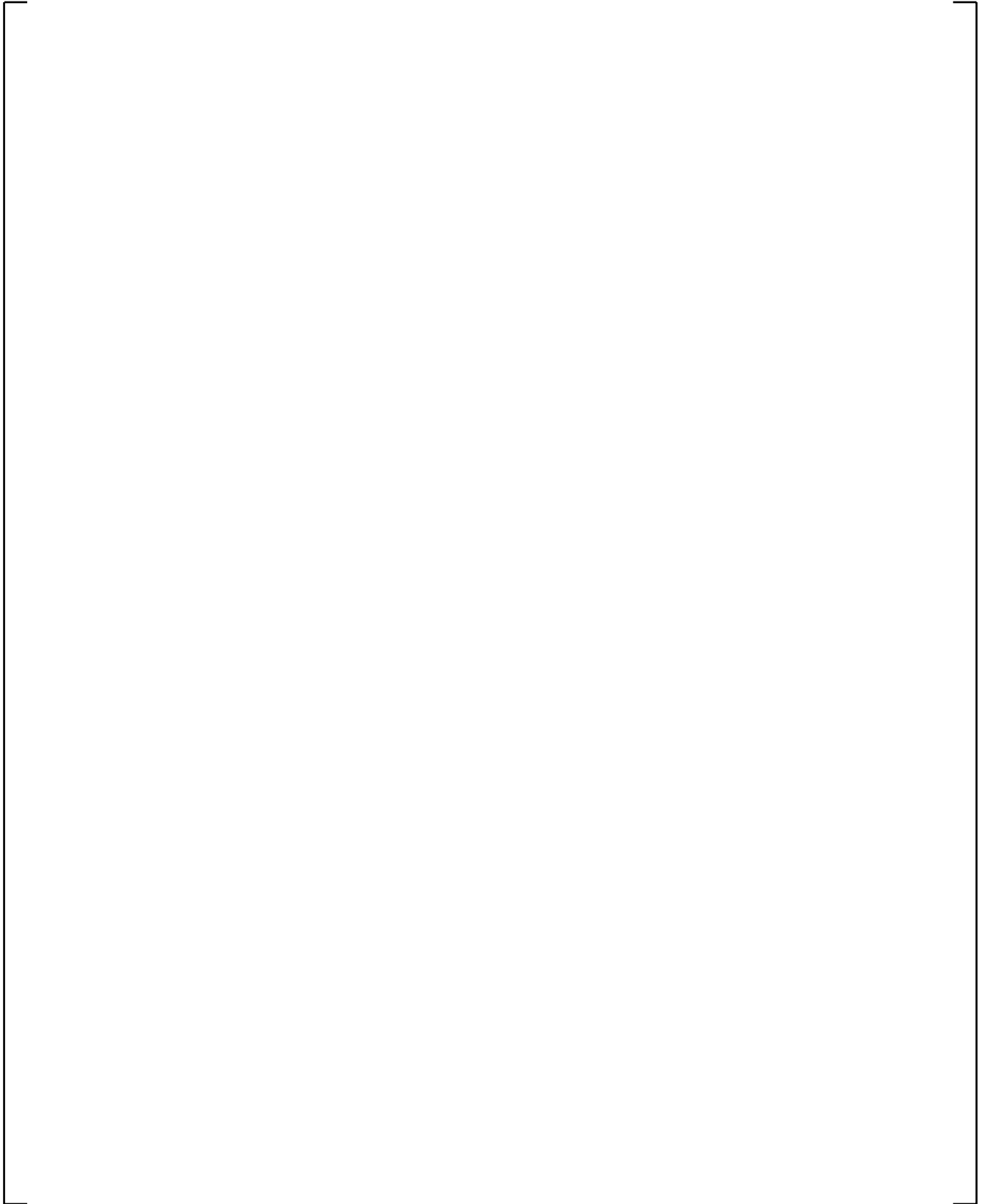
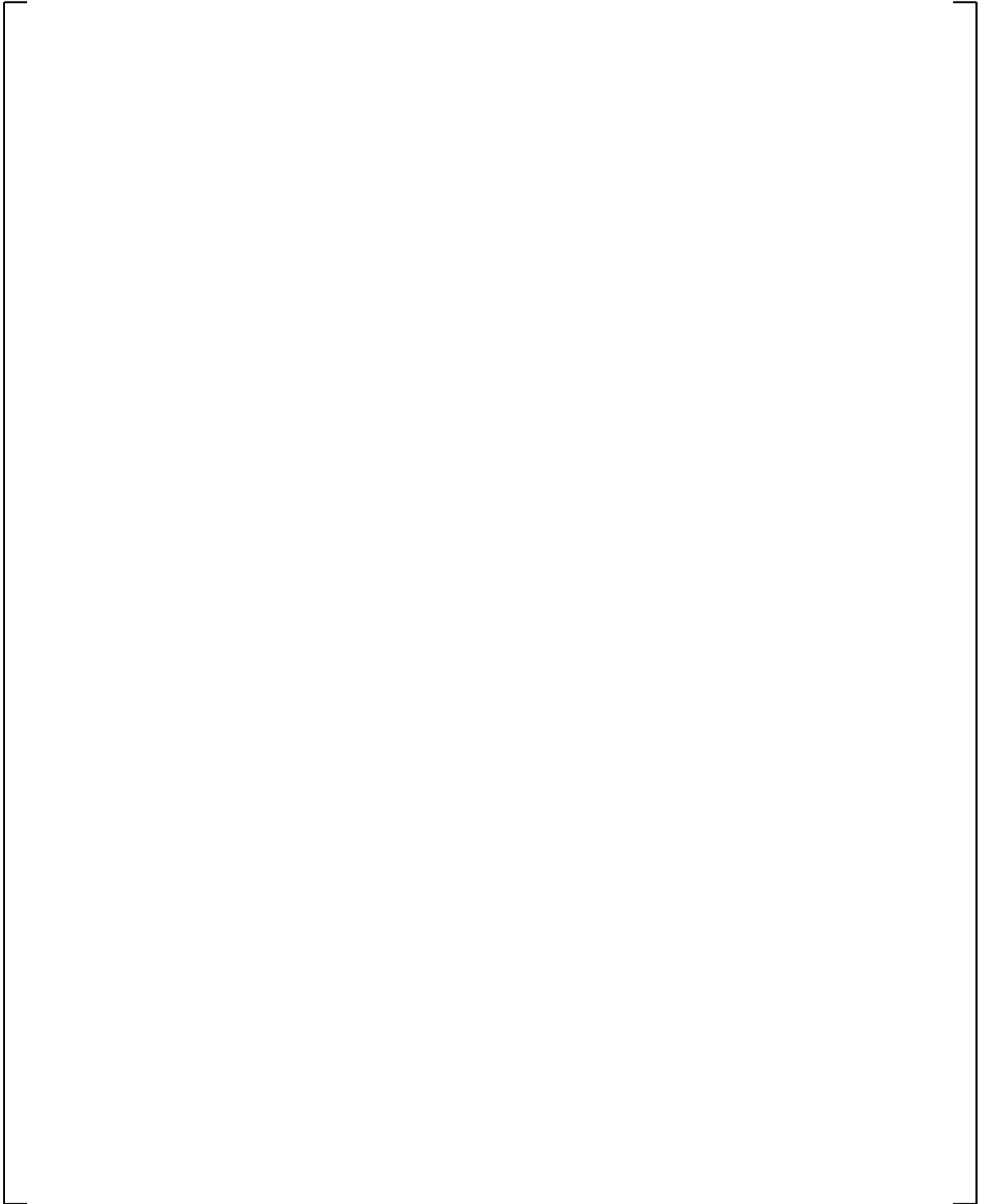**Figure 3.2-42   Axial Power Distribution (Plant A, Cycle 8)**

Figure 3.2-43   Axial Power Distribution (Plant A, Cycle 9)
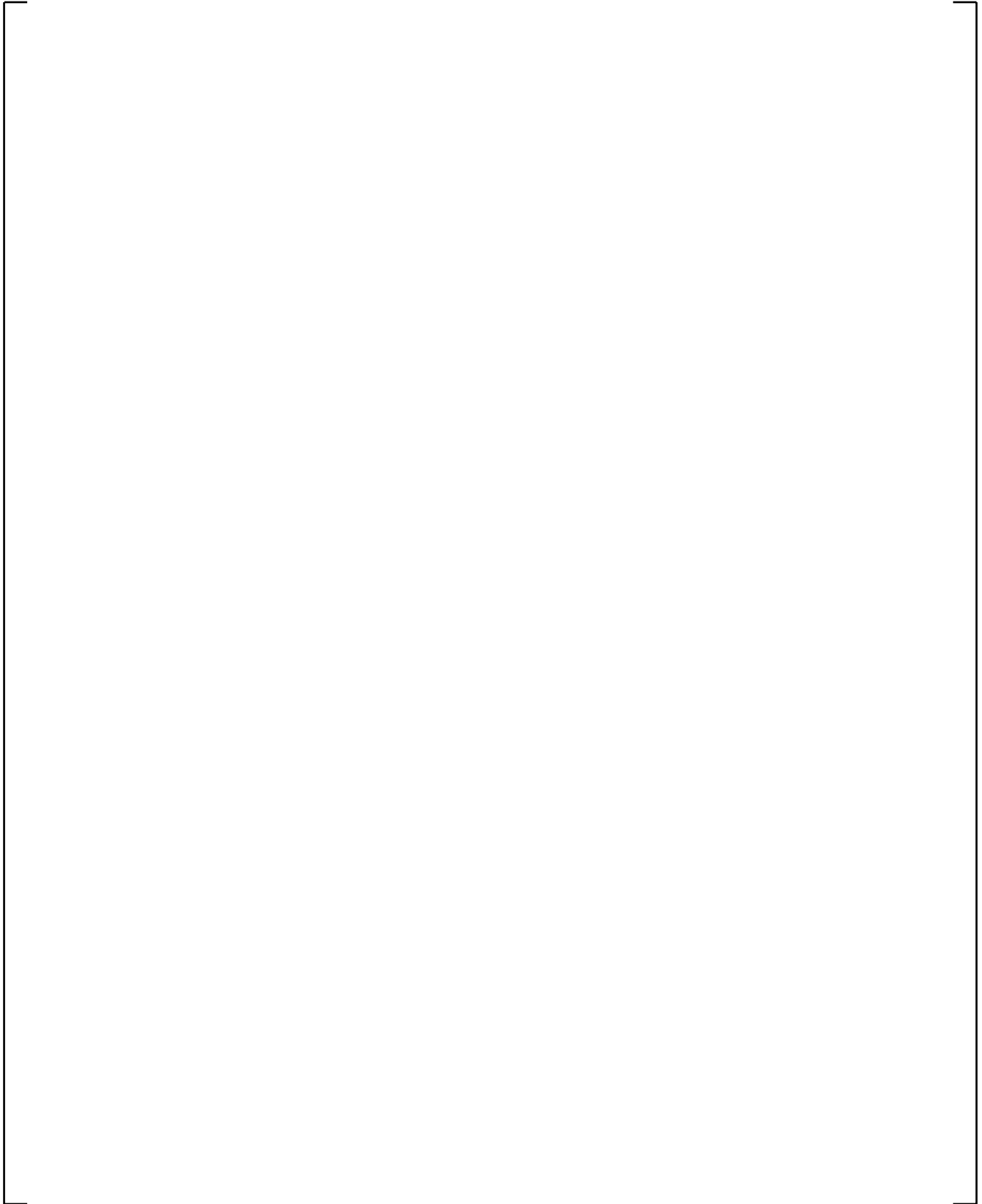
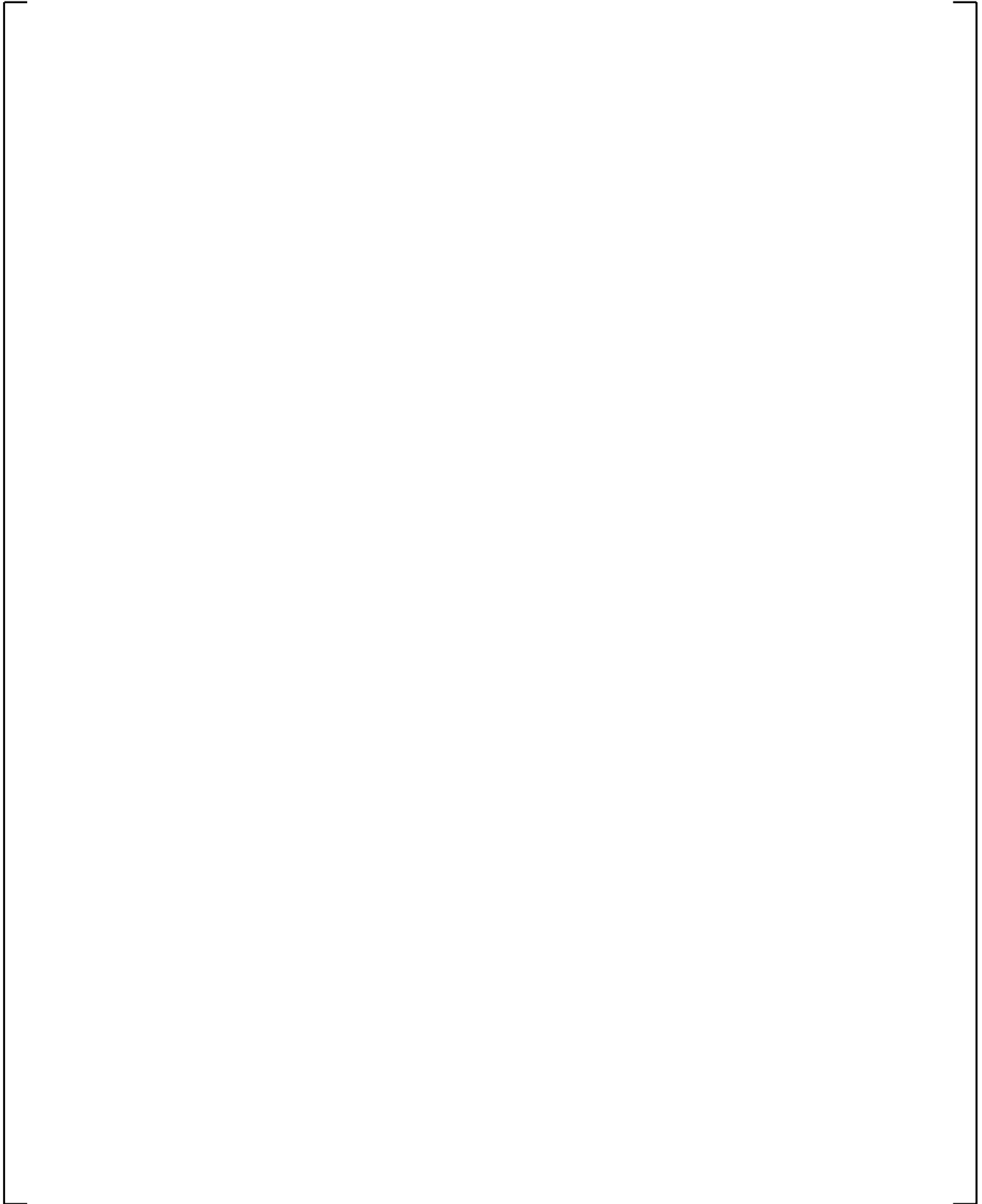**Figure 3.2-44   Axial Power Distribution (Plant B, Cycle 6)**

Figure 3.2-45   Axial Power Distribution (Plant B, Cycle 7)
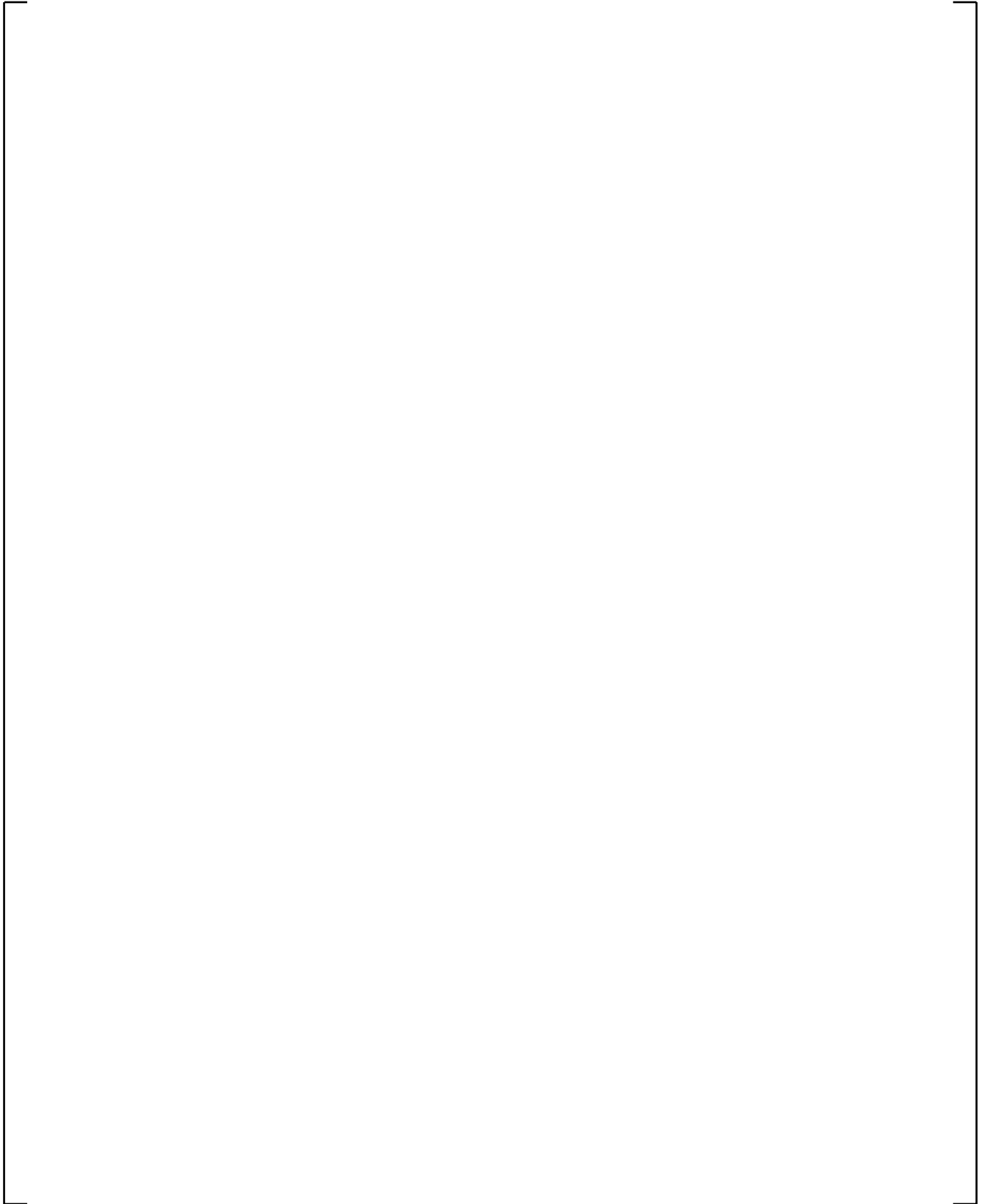
Figure 3.2-46   Axial Power Distribution (Plant B, Cycle 8)

4.0   CONCLUSIONS

MHI has constructed 23 Westinghouse type standard PWRs in Japan. Additionally, MHI has experience in the design of over 400 reload cores, including 19 initial cores. MHI has extensive experience in construction, design, core reload and core performance improvement of PWR plants. This document provides the results to show the capability of MHI PWR nuclear design methodology using PARAGON/ANC.

PARAGON/ANC is a code system approved by NRC. MHI introduced this code system from WH. Furthermore, since the 1990s and for over 10 years, MHI and WH have implemented joint development programs in order to develop and improve this code system. MHI has been using this code system in the core analysis of the Japanese PWRs.

The qualification of MHI PWR nuclear design method using PARAGON/ANC has been performed by comparing the code system results with measurement data from critical experiments, PIE and operating plants. As for the critical experiments analyses, experiments using UO_2 and MOX fuel rods have been analyzed by using the PARAGON code and confirming the good performance of this code. To confirm the applicability of PARAGON for the US-APWR neutron reflector, critical experiments using an iron reflector has been performed. The comparison between PARAGON calculated results and measurements shows good agreement. For the PIE analyses, the measurement isotopic data of UO_2, MOX, and high-content Gadolinia fuel rods were compared to PARAGON calculated results. The PARAGON results shows a good agreement with experiment results and no particular trends between PARAGON and measurements results for any isotope with burnup or Gadolinia contents. For the operating plant analyses, 10 cores of 2 plants including initial and reload cores with high content Gadolinia and extended burnup UO_2 fuel have been analyzed. The comparison between PARAGON/ANC calculated results and the startup physics tests and HFP operating measurement data shows good agreement. There are no particular trends between PARAGON/ANC calculated results and measurements for any core characteristics with plant type, core type, cycle burnup, and other core parameters.

As a result of these analyses, the good performance of the PARAGON/ANC code system demonstrates the ability of the MHI to apply PWR nuclear design methodology using PARAGON/ANC.

5.0   REFERENCES

1.   Ouisloumen, M. et al., Qualification of the Two-Dimensional Transport Code PARAGON, WCAP-16045-P-A (Proprietary), and WCAP-16045-NP-A (Non-Proprietary), August, 2004.

2.   Liu, Y. S., et al., ANC – A Westinghouse Advanced Nodal Computer Code, WCAP-10965-P-A (Proprietary), and WCAP-10966-A (Non-Proprietary), September, 1986.

3.   Nguyen, T. Q., et al., Qualification of the PHOENIX-P/ANC Nuclear Design System for Pressurized Water Reactor Cores, WCAP-11596-P-A (Proprietary), and WCAP-11597-A (Non-Proprietary), June, 1988.

4.   Strawbridge, L. E., and Barry, R. F., Criticality Calculations for Uniform Water-Moderated Lattices, Nucl. Sci. Eng. 23, 1965.

5.   Persson, R., Blomsjo, E., and Edenius, M., High Temperature Critical Experiments with H_2O Moderated Fuel Assemblies in KRITZ, Technical Meeting NO. 2/11, NUCLEX 72, 1972.

6.   Mosteller, R. D., Critical Lattices of UO_2 Fuel Rods and Perturbing Rods in Borated Water, LA-UR 95-1434, 1995.

7.   Newman, L.W., Urania-Gadolinia: Nuclear Model Development and Critical Experiment Benchmark, DOE/ET/34212-41, April, 1984.

8.   MCNP4B – Monte Carlo N-Particle Transport Code System, CCC-600, RSICC Computer Code Collection, April, 1997.

9.   Baldwin, M. N., Physics Verification Program Part III, task 11 Quarterly Technical Report July-September 1974, BAW-3647-30, July, 1974.

10. Charlier, A., et al., VENUS International Program (VIP) A Nuclear Data Package for LWR Pu Recycle, Proc. Int. Conf. on the Physics of Reactors: Operation, Design and Computation MARSEILLE-FRANCE, 1990.

11. Suyama, K., et al., Improvements to SFCOMPO – a Database on Isotopic Composition of Spent Nuclear Fuel, JAERI-Conf 2003-019, 2003.

12. Lippens, M., et al., Source Term Assessment : The ARIANE Programme, ICEM'01 the 8th Int. Conf. on Radioactive Waste Management and Environment Remediation, 2001.

13. Lippens, M., GAP FINAL REPORT, 1990.

14. Murakami, K., et al., Measurement of reactivity effect for iron plate reflector in light-water moderated low enriched UO_2 lattices, JAERI-M 83-100, 1983.

15. Tahara, Y., et al., <u>Reactivity Effect of Iron Reflector in LWR Cores</u>, Journal of NUCLEAR SCIENCE and TECHNOLOGY, Vol. 38, No. 2, p. 102-111, February, 2001.

16. American National Standard <u>Reload Startup Physics Tests for Pressurized Water Reactors</u>, ANSI/ANS-19.6.1-2005.